Biosensors and Bioelectronics 127 (2019) 215–220

Contents lists available at ScienceDirect

Biosensors and Bioelectronics

journal homepage: www.elsevier.com/locate/bios

Field effect in molecule-gated switches and the role of target-to-receptor size ratio in biosensor sensitivity

Beatriz L. Garrote, Flavio C.B. Fernandes, Eduardo M. Cilli, Paulo R. Bueno*

Institute of Chemistry, São Paulo State University (UNESP, Universidade Estadual Paulista), CP 355, 14800-060 Araraquara, São Paulo, Brazil

ARTICLE INFO

Keywords:
Quantum capacitors
Redox switches
Debye screening
Thomas-Fermi screening
Molecular transistor
Molecular electrochemistry

ABSTRACT

We demonstrated here that molecular redox films are electrochemical capacitive devices possessing specific field effect in which molecular moieties within films act as sensitive gates. We confirm that the field effect present in these redox switches is suitable in detecting, in a label-free manner (without needs of redox probe in the biological samples), biomarkers of essential importance for dengue, heart risks and inflammation, Parkinson's disease and tumors. Though the sensitiveness is high, it is governed by Thomas Fermi screening and thus depends on the target-to-receptor size ratio. Thus, we also demonstrated how this target-to-receptor size ratio affects the sensitivity. We concluded that the smaller the biological receptor the greater the sensitivity. Consequently, a larger molecular target associated with a smaller receptor provides a considerable (predictable) improvement of the sensitiveness.

1. Introduction

Transistors (Ariga et al., 2007; Chen et al., 2012, 2007; Grieshaber et al., 2008; Gudiksen et al., 2002; Hanafi et al., 1996; McAlpine et al., 2007; Singh et al., 2011; Wang, 2004) are devices that serve to amplify or switch electronic signals and electrical power. Field effect transistors (FET), which use electric fields to control the behavior of the device, are typically made of three terminals, i.e., source (S), drain (D) and gate (G) (see Fig. 1a). Conductivity between the drain and source terminals is controlled by an electric field induced in the device, which is generated by the differences in voltage between the channel and gate terminals. Chemically sensitive field effect transistors (Balasubramanian and Burghard, 2006; Bartic and Borghs, 2006; Vanderspiegel et al., 1983) measure chemical alterations based on electric field variations in the chemically reactive environment in which they are embedded. For instance, when the concentration of a target analyte in a solution (in contact with the channel) is varied, the electric current through the transistor responds accordingly. Variations in the concentration of charged analyte ions in the solution induce a chemical potential difference between the source and gate, which is measurable by the FET as a change in the electric current. This transistor design is known as electrolyte-gated FET (Ohno et al., 2009; Rosenblatt et al., 2002), because the ions do not penetrate into the channel, but instead accumulate near its surface or near the surface of a dielectric layer (deposited on the channel), inducing charge accumulation inside the channel, which is thus probed by electric field variations near and through the surface.

Organic electrochemical transistors (OECT) (Berggren and Richter-Dahlfors, 2007; Bondy and Loeb, 2003; Friend et al., 1999; Kaempgen et al., 2009; Lange et al., 2008; Lin and Yan, 2012; Mabeck and Malliaras, 2006; McCulloch et al., 2006) are a category of chemically sensitive FET in which the drain electric current is controlled by the injection of ions from an electrolyte into the channel, thereby altering the electronic charge density throughout its entire volume, which provides a very high transconductance. The disadvantage of OECTs is that, albeit sensitive, they are slow. The electronic properties in both electrolyte-gated FET and OECT are controlled by ionic movement, and hence, by non-faradaic characteristics of the interface (Bartic and Borghs, 2006; Lin and Yan, 2012). The non-faradaic charge characteristics at the interface are governed by double layer capacitance and Debye field effect screening, following the Debye length scale.

Our goal is to classify redox switches as organic electrochemical devices that possess field effects that could be used to sensor, called mesoscopic organic electrochemical field effect sensors (MOEFES). The nature of this category of field effect device is intrinsically mesoscopic (Fig. 1b), combining classic and quantum mechanics effects inside channel and gate components of the device. One of the advantages of using electrochemical capacitive biosensors, as a type of MOEFES, is that they are label-free and highly sensitive [femtomolar sensivities (Marques et al., 2015) are possible to be reached in some cases] and

* Corresponding author.
E-mail address: paulo-roberto.bueno@unesp.br (P.R. Bueno).

https://doi.org/10.1016/j.bios.2018.12.018
Received 3 December 2018; Accepted 7 December 2018
Available online 13 December 2018
0956-5663/ © 2018 Elsevier B.V. All rights reserved.

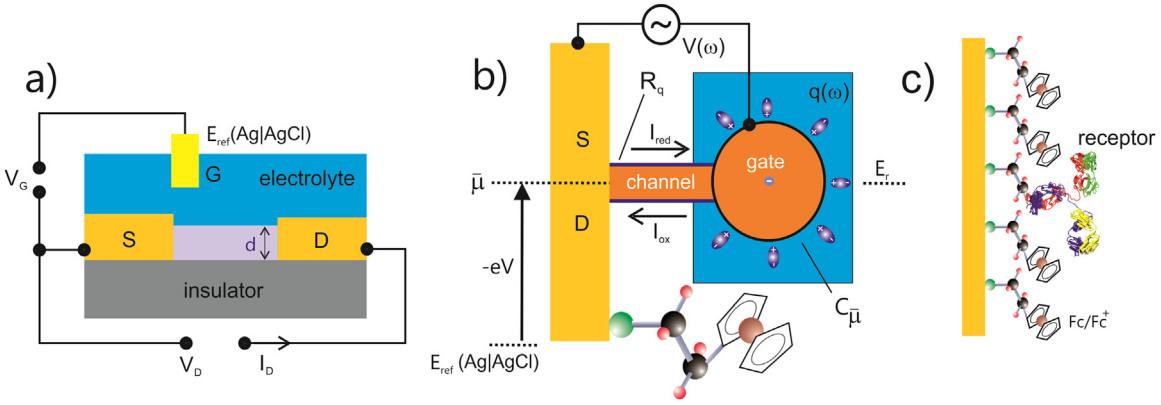

Fig. 1. a) Typical architecture of an electrolyte-gated and organic chemically sensitive FET, where E_{ref} corresponds to the electrochemical (silver/silver chloride) reference electrode, d is the thickness of the organic (or dielectric) layer permeable to ions in contact with an electrolyte. b) Schematic representation of a mesoscopic electrochemical field effect of molecular architecture using redox switches, i.e., ferrocene-terminated alkane thiols (alternatively, a redox-active peptide chain can be used (Piccoli et al., 2018), see below). The molecular chain linking the switch to the electrode acts as a tunneling channel. Ferrocene is generally used as the redox capacitive switch. a) and b) are examples of electrochemical transistors, but b) is dominated by physical mesoscopic effects. c) Illustration of redox switches alkane thiol monolayers assembled on metallic electrodes within receptors.

additionally do not require the use of redox probe in solution or any other chemical reagents are needed to be added to the patient's samples before assaying. See more details about the advantages of using electrochemical capacitive sensors in Supplementary material; section SM.1, where we also mention about their advantages in terms of multiplex abilities and applications in point-of-care platforms. Part of the high sensitivity is due to the fact that the capacitive signal is associated with field-effect as will be discussed in detail further here. As Fig. 1b shows, the electric field in a MOEFES is screened following redox dynamics. In other words, the dynamic equilibrium of the electrochemical current (oxidative and reductive), termed exchange current (Bard and Faulkner, 2000), is resonant with electronic states contained in the electrode. The associated electrochemical capacitance, $C_{\bar{\mu}}(\omega) = dq(\omega)/dV(\omega)$, which is frequency dependent, can be determined by impedance-derived capacitance measurements (Bueno et al., 2016). Note that the source and drain electric current contributions depend on the steady state bias $dV = d\bar{\mu}/e$ imposed by a potentiostat. The electrochemical equilibrium of the mesoscopic field effect structure occurs at $\bar{\mu} = E_r$, i.e., when $\bar{\mu}$, which is the electrochemical potential of the electrons in the electrode, is energetically aligned with E_r, which in turn is the formal potential of the redox switch. Accordingly, the Fermi level is constant at the junction, meaning that there is no electron net flux despite the presence of a dynamic resonant current (see Fig. 1b).

Our aim here is to demonstrate that a molecular film comprising redox active switches operates as a MOEFES. We show that $C_{\bar{\mu}}$ governs the electrical field screening of the switches (Bueno et al., 2016; Bueno and Davis, 2014a, 2014b; Eckermann et al., 2010) and that the target-to-receptor size ratio (coupled to the switch's gate) modulates the signal sensitivity of MOEFES, as designed for applications in molecular diagnostics (Bradley et al., 2004; Cecchetto et al., 2015, 2017; Fernandes et al., 2013; Lehr et al., 2014; Santos et al., 2014, 2015).

2. Material and methods

2.1. Chemical reagents

1-Ethyl-3-(3-dimethylaminopropyl) carbodiimide (EDC), N-hydroxysuccinimide (NHS), perchlorate tetrabutylammonium (TBA-ClO_4), 16-mercaptohexadecanoic acid (16-MHDA) and 11-ferrocenyl-undecanethiol (11-FcC) were purchased from Sigma-Aldrich. Human C-reactive protein (CRP) and human CRP polyclonal antibody (Ab) were also purchased from Sigma-Aldrich, while interleukin-6 (IL-6) and IL-6 Ab were purchased from Rhea Biotech. Alpha-synuclein (α-sync) protein and α-sync Ab were purchased from Santa Cruz Biotechnology, and the recombinant dengue virus non-structural 1 (NS1) protein and monoclonal antibody (ab64456) were purchased from Abcam.

The peptide used as support of some for the receptors was Fc-Glu-Ala-Ala-Cys, manually synthesized by solid phase peptide synthesis using Fmoc protocols on rink amide resin (0.48 mmol g^{-1}). Coupling was performed at a 2-fold molar excess relative to the amino component in the resin, using diisopropylcarbodiimide (Dic)/ 1-hydroxybenzotriazole (HOBt). Fmoc groups were deprotected using 20% 4-methylpiperidine/dimethylformamide (DMF) for 80 min. The ferrocene redox probe was introduced at the N-terminus by reaction with one molar equivalent 3-ferrocenylpropionic anhydride in 5 mL DCM/DMF (1:1) for 24 h. Peptide cleavage was performed by removing side chain protecting groups with 94% trifluoroacetic acid (TFA), 2.5% 1,2-ethanedithiol, 2.5% H_2O and 1% triisopropylsilane for 2 h. The peptide was then precipitated with diethyl ether and separated from the reaction solution by centrifugation. Further details of the synthesis are given in reference (Piccoli et al., 2018).

Phosphate buffered saline (PBS) was prepared using the following salt concentrations: 8 g L^{-1}NaCl, 0.2 g L^{-1} KH_2PO_4, 1.15 g L^{-1} $NaH_2PO_4{\cdot}12H_2O$, 0.2 g L^{-1}KCl, and 0.2 g L^{-1} $NaNO_3$, reaching an expected pH of 7.4.

2.2. Brief description of receptors and target biomarkers

CRP is a protein synthesized by the liver. CRP exists in the form of pentamers with identical protomers, leading to a ~ 118 kDa protein. CRP, which is present in the blood of healthy individuals, serves as biomarker of inflammation caused by infection or injury, hypertension and cardiovascular diseases. Serum CRP levels exceeding 3.0 mg L^{-1} are indicative of risk of diabetes. NS1 is a 46 kDa non-structural protein of *Flavivirus* widely used to diagnose dengue (Parkash and Hanim Shueb, 2015). In the first week after the onset of Dengue symptoms, NS1 can be detected in a concentration (Alcon et al., 2002) of 0.04–2.00 μg mL^{-1} in serum. Alpha-sync, a protein predominantly expressed in neural tissue, is essential for synaptic functions by augmenting transmitter release from the presynaptic terminal. Dysfunctional regulation of α-sync is directly related to the pathogenesis of Parkinson's disease. Alpha-sync antibodies interact strongly with different epitopes of this protein and have different specificities towards different oligomers of α-sync, and their use as a receptor is a matter of controversy. Thus, we used α-sync as a receptor in order to detect its antibody, enabling us to evaluate the effect of a small receptor (14.4 kDa, α-sync) to detect a larger target (150 kDa, the α-sync Ab). Human IL-6 is a 26 kDa

glycoprotein and a member of the cytokine family, which affects the functionalities of the immune system. It is involved in the differentiation process of myeloid cells and in homeostatic and neuroendocrine functions. (Barton, 1997) The overexpression of IL-6 is associated with cardiovascular disease, osteoporosis, diabetes, arthritis and tumors. Increasing interest has focused on the association of IL-6 with cardiovascular disease. This is the first attempt at detecting IL-6 using an impedance spectroscopic method.

The electrode pretreatment, electrochemical measurements and fabrication of the biosensing interface are detailed in the Supplementary material.

3. Results and discussion

3.1. Electrochemical capacitance and electric field screening

We recently demonstrated that physical and chemical concepts at the nanoscale are unified for electronics and electrochemistry based on the meaning of $C_{\bar{\mu}}$ (Bueno, 2018). Theoretical and experimental investigations into the impedance of redox-active switches reveal that the timescale is controlled by quantum resistive-capacitive characteristics. The implication is that the electrochemical reaction rate in these switches is governed by $k = 1/R_q C_{\bar{\mu}} = G/C_{\bar{\mu}}$, where $G = 1/R_q$ is a quantized conductance (Landauer, 1992) acting as a quantum channel connecting the molecular switches to the macroscopic electrode, as depicted in Fig. 1b. If an interface containing an ensemble of individual capacitive switches is arranged with receptors upon it (Fig. 1c), a sensorial interface is constructed (Bueno et al., 2017). The sensitivity of the binding of a target analyte to the receptor can be monitored by measuring $C_{\bar{\mu}}$, because the electrochemical potential at the gate of the switches varies in the presence of a bond between receptor and target. This variation is triggered by $C_{\bar{\mu}}$. $C_{\bar{\mu}}$ is a series contribution of two different capacitances, such as: (Bueno et al., 2015; Büttiker et al., 1993)

$$\frac{1}{C_{\bar{\mu}}} = \left(\frac{1}{C_i} + \frac{1}{C_q}\right) \tag{1}$$

where C_i is the ionic capacitance of the interface (Hudari et al., 2018) (normally modeled by double layer capacitance) and $C_q = e^2\mathcal{N}$ is the quantum capacitance associated with the accessible electrochemical density of states (Bueno and Davis, 2014b; Bueno et al., 2017), $\mathcal{N}$, within the switches. Eq. (1) predicts double layer capacitive effects and also considers quantum capacitive effects associated with the charge of the electronic states of the switches, which includes consideration of Thomas-Fermi electrical field screening, where $\kappa = (C_{\bar{\mu}}/\varepsilon_r\varepsilon_0)^{1/2}$ is the Thomas-Fermi wave vector. The length scale associated with the Thomas-Fermi wave vector rules the potential decay related to the screening of the electric field (Gutierrez et al., 2017; Lehr et al., 2017).

The dominance of Thomas-Fermi over Debye screening is thus a matter of electronic control over ionic dynamics to accommodate electric field variations as a function of redox modifications prevailing at the interface. Both ionic (distinguishable particles) and electron (indistinguishable particles) dynamics are engrained in experimentally resolved $C_{\bar{\mu}}$ of the switches. For instance, assuming a Boltzmann approximation and considering that screening is governed by ions (in a pure non-faradaic charge at the interface), then $\mathcal{N} \propto \exp[-eV/k_BT]$ corresponds to the concentration of the ions in the bulk solution, where k_B is the Boltzmann constant and T is the absolute temperature. Thus, Debye length can be determined from the Thomas-Fermi wave vector, recovered as $\kappa = [(2e^2\mathcal{N})/(\varepsilon_0\varepsilon_r k_B T)]^{1/2}$ and embedded in the Debye-Hückel model (Grosberg et al., 2002; Levin, 2002), which demonstrates that the double layer phenomenon is only an approximation of Eq. (1) (Lehr et al., 2017). On the other hand, upon assuming a pure faradaic charge at the interface, governed by electron dynamics only so $\mathcal{N} \propto (1+\exp[-eV/k_BT])^{-1}$, $\mathcal{N}$ now corresponds to the electrochemical density of states associated with the C_q term and the fluctuation of electric potential is distributed according to Fermi-Dirac statistics, no longer following Boltzmann considerations.

In summary, both faradaic and non-faradaic electrochemical processes are approximations of an identical mesoscopic effect governed by ionic or electronic dynamics. The mesoscopic model, as predicted in Eq. (1), incorporates the two effects realistically. Electrolyte-gated FETs and OECTs are ruled by Debye screening while, remarkably, MOEFES can be designed to follow Thomas-Fermi screening.

3.2. Mesoscopic electrochemical transistors and electrochemical capacitance

We will now demonstrate that Eq. (1) complies with the design of switchable FETs in the equilibrium state and that MOEFES can be ruled solely by Thomas-Fermi screening. Let us begin by considering that the potential difference between redox switchable gates and the electrode is V_G, onto which a sinusoidal perturbation, $V(\omega)$, is applied (see Fig. 1b) to attain the impedance. The potential in the quantum channels, V_c, is dependent on the electron density in the channels, N_c, such as

$$V_c = V_G - eN_c/C_i, \tag{2}$$

where $q_c = eN_c$ is the charge in the channels and eN_c/C_i is the potential of electrons in the channel electrostatically equilibrated by the electrolyte. The capacitance in the gate can therefore be written as $dq_c/dV_G = (dq_c/dV_c)(dV_c/dV_G)$. Now, by applying the derivative of Eq. (2) with respect to V_G, one reaches $dV_c/dV_G = 1 - [(1/C_i)(dq_c/dV_G)]$, and thus, Eq. (2) can be rewritten as

$$\frac{dq_c}{dV_G} = \frac{dq_c}{dV_c}\left(1 - \frac{1}{C_i}\frac{dq_c}{dV_G}\right). \tag{3}$$

By assuming that dq_c/dV_G is the equivalent capacitance, i.e., the $C_{\bar{\mu}}$ of the system, and noting that dq_c/dV_c is the quantum capacitance, C_q, we thus obtain

$$\frac{1}{C_{\bar{\mu}}} = \frac{dV_G}{dq_c} = \left(\frac{C_q + C_i}{C_q C_i}\right) = \frac{1}{C_i} + \frac{1}{C_q}. \tag{4}$$

The capacitance of the gate is thus governed by $C_{\bar{\mu}}$,and notably, Eq. (2) is recovered, *quod erat demonstrandum*. The inverse of $C_{\bar{\mu}}$ thus drives the field effect, which demonstrates, by experimentally accessing $C_{\bar{\mu}}$, that the thermodynamic properties of the redox switches are traceable, so that molecular changes are perceptible. It should be noted that the analysis of energy storage (Miranda and Bueno, 2016) in redox switches leads to $E = q^2/2C_{\bar{\mu}}$, where q is the electric charge. Variations in this energy due to the occupancy of the quantum states within $C_{\bar{\mu}}$ are reported through derivatives of E with respect to the charge (Luryi, 1988), resulting in $dE/dq = q/C_{\bar{\mu}}$, which is explicitly associated with a ΔV_G, from where field effects can be monitored.

We now will provide experimental evidence that corroborates the aforementioned concepts. Our aim, in particular, is to show how the "size" ratio of the target to receptor is coupled to molecular switches. This ratio impacts $\kappa^{-1} = (\varepsilon_r\varepsilon_0/C_{\bar{\mu}})^{1/2}$, which is the length scale that governs sensitivity.

3.3. Experimental validation of the field effect and mechanisms controlling the sensitiveness

Fig. SM1 shows the variation in $C_{\bar{\mu}}$ of an interface comprising CRP Ab receptors bonded on 16-MHDA/11-FcC, serving as a MOEFES to monitor neighboring CRP recognition. The MOEFES architecture provides a comparable magnitude of $C_{\bar{\mu}}$ signal, no matter what type of molecular construction (peptide or alkane thiols) is used to anchor the switches to the electrode. Also, the limit of detection (LoD) obtained for the detection of CRP by capacitive methods are in between 5 and 250 pM and compares quite favorably to other methods (Bing and Wang,

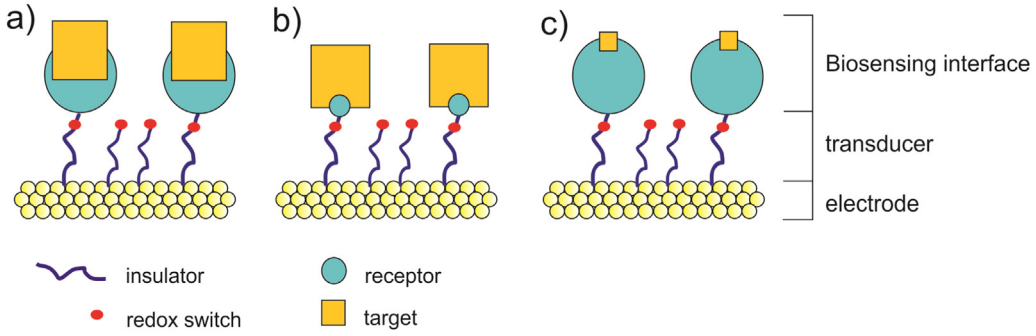

Fig. 2. This figure illustrates the conformations and structural configurations to design a mesoscopic organic electrochemical transistor using redox switches as gates, receptors and targets (as assay components) of different size ratios. Since sensitivity is controlled by the range of the field effect, which in turn is governed by the length scale associated with $1/C_{\bar{\mu}}$, then: a) illustrates cases where an intermediate sensitivity is predicted, while b) illustrates the best expected sensitivity, and c) shows the worst.

Table 1
Influence of the molecular weight of the target on the system's sensitivity. Assays based on 16-MHDA/11-FcC mixed molecular layers.

	Target	Molecular weight (kDa)	Sensitivity [% (mol L^{-1})][a]
Cecchetto et al. (2017)	NS1	46	14
Fernandes et al. (2015)	CRP	118	30
	α-sync Ab	150	84

[a] Sensitivity obtained from the slope of the analytical curve expressed as a relative response (RR) per decade of antigen.

Table 2
Influence of the target's molecular weight and the receptor rate on the system's sensitivity. Assays based on redox peptide monolayers.

	Target	Target molecular weight (kDa)	Receptor molecular weight (kDa)	Sensitivity [% (mol L^{-1})][a]
Fernandes et al. (2015)	α-sync Ab	150	14.4	84
Piccoli et al. (2018)	CRP	118	150.0	11 ± 1
	CRP	118	~ 2.0	88 ± 4

[a] Sensitivity obtained from the slope of the analytical curve expressed as a relative response (RR) per decade of antigen.

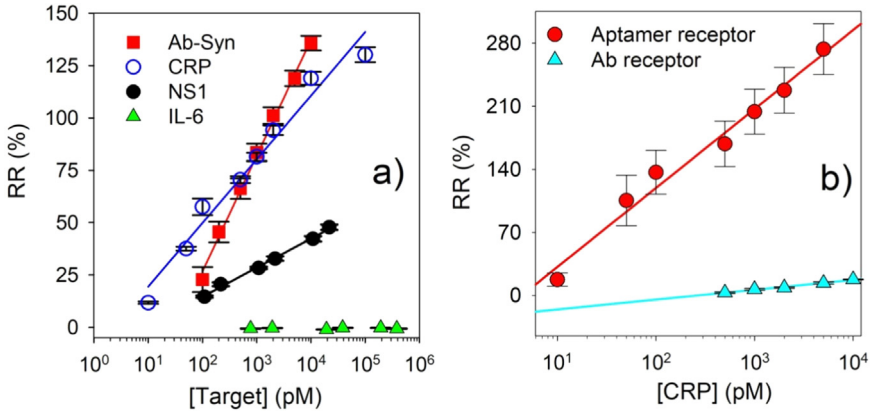

Fig. 3. a) Analytical curves showing the sensitivity achieved for different target-to-receptor size ratios. b) The same as in a), but comparing how different (aptamer or antibody) receptor sizes respond to the same target (CRP).

Table 3
Sensitivity and target-to-receptor "size" ratio. Pep and FcC are abbreviations for the receptor anchored on peptide or alkane thiol layers.

Interaction	Ratio (target/receptor)	Sensitivity [% (mol L^{-1})][a]
IL-6_{pep} Ab /IL-6	0.17	–
$NS1_{FcC}$ Ab/NS1	0.30	14
CRP_{pep}Ab/CRP	0.79	11
CRP_{FcC}Ab/CRP	0.79	30
α-$sync_{FcC}$/α-sync Ab	10.41	84
DNA_{pep}/CRP	59.17	88

[a] Sensitivity obtained from the slope of the analytical curve expressed as a relative response (RR) per decade of antigen.

2017; de Ávila et al., 2013; Guo et al., 2018; Yang et al., 2014) in which the lowest LoD reported was c.a. 180 pM (Bing and Wang, 2017). As described in the experimental section and Supplementary material, the molecular coverage is directly proportional to the capacitance and was carefully taken into account in this analysis where they are same for the different redox switch films. One could argue that the target binding is offsetting the reversible potential, but is not the case as we demonstrated previously (Bueno et al., 2017). There is no change in the reversible or formal potential of the electrode as targeting is binding to the receptors (see Fig. 2b of reference (Bueno et al., 2017)).

In Table 1, note the explicit effect of the molecular weight of the target protein on the sensitivity when using solely ferrocene-terminated alkane thiols. The higher the molecular weight the greater the sensitivity. The intrinsic transducer characteristics of the $1/C_{\bar{\mu}}$ signal and the associated Thomas-Fermi electric field screening characteristics

enabled us to determine how sensitivity operates in redox-active molecular films. Assaying CRP, NS1, α-sync Ab (Fernandes et al., 2015) and IL-6 requires biological receptors of different molecular weights. For CRP assays, CRP Ab, a molecule of 150 kDa, was used as the receptor (Fernandes et al., 2015), whereas for α-sync Ab assays a receptor possessing a molecular weight of 14.4 kDa (Fernandes et al., 2015) was used. The capacitive sensing for α-sync Ab showed three-fold higher sensitivity than for CRP-Ab/CRP assays.

Differences in the performance of the assay to detect CRP and α-sync Ab are related to the electrochemical potential [$\Delta V_G = \Delta(q/C_{\bar{\mu}})$] triggered by variations associated with changes in the electron occupancy of the switch, as induced by variations in the chemical potential at the interface. Thus, the results described in Table 1 and 2 are interpreted based on variations (Bueno et al., 2015) in the occupancy of the switch, which depend on the response of the electronic structure of the interface to variations in the chemical environment, according to Eq. (1). When this faradaic interface is electrochemically interrogated and variations in $C_{\bar{\mu}}$ are tracked, it is predicted that the higher the molecular weight of the target, the greater the impact of variations in the chemical potential at the interface, thus proportionally affecting the redox activity and the occupancy of the electrochemical states. In other words, the impact of variations in the target's chemical potential induced by the receptor size (inferred from the molecular weight) is recognized by the redox switches through variations in the field effect related to $C_{\bar{\mu}}$, according to the equivalence between Eqs. (1) and (4), which confirms that the switches actually act as quantized electrochemical gates (Bueno and Davis, 2014b; Bueno et al., 2017).

Our search on biosensors in the literature found no previous work demonstrating label-free capacitive resolutions at the molecular level such as those addressed here. This means that the field effect characteristics of MOEFES can now be evaluated in depth. The distance between the biological recognition center and the switch gate, whose possibilities are illustrated in Fig. 2, is presumably an important factor. It is the range of the electric field, or the range of the electrochemical potential of the redox gates, that governs the sensitivity. The target-to-receptor size ratio serves as an estimate of the range to be attained by the electric field, which is herein inferred from the ratio between the molecular weight of the target and that of the receptor.

Tables 1, 2 (and Fig. 3, visually) show the variances between the molecular weights of receptor and target obtained in different assays. Piccoli et al. (2018) work (Table 2) reported on the sensitivity of different molecular weights of the receptors (CRP Ab and CRP DNA aptamer) to sense the CRP target. Not surprisingly, the relative percent response of the variation of $1/C_{\bar{\mu}}$ as a function of CRP concentration, using CRP Ab (11 ± 1) as receptor, was almost eight times lower than the homologue receptive aptamer (88 ± 4). Because of the length scale of the $1/C_{\bar{\mu}}$ signal range, the smaller the biological receptor the greater the sensitivity. Consequently, a larger molecular target associated with a smaller receptor provides a considerable improvement in sensitivity.

To confirm the hypothesis that sensitivity is associated with field effect characteristics and length scales of the capacitive signal, we took the redox peptide switch used in the work of Piccoli et al. (2018) as the molecular layer to support a receptor of the largest possible size.

The receptor, the Ab IL-6 protein of 150 kDa, could therefore not reasonably sense a small target IL-6 of only 26 kDa (see Fig. 3), i.e., the smallest possible target-to-receptor size ratio of this work (Table 3). The larger receptor caused a significant impediment preventing the capacitive signal of the switch from sensing the target. Hence, the range of the electrochemical potential of the redox gates was no longer suitable for detecting the binding event. In fact, the IL-6 Ab used as a receptor to detect IL-6 is the smallest target-to-receptor size ratio our research group has tested so far. Accordingly, the molecular weight of IL-6 was, comparatively, 1.8-fold lower than NS1, 4.5-fold lower than CRP and 5.8-fold lower than α-sync Ab targets. Note that albeit the ratio of $CRP_{pep}Ab/CRP$ and $CRP_{FcC}Ab/CRP$ is the same because both assays have the same receptor and target (i.e. antibody for CRP and CRP), the slight difference observed in their sensitivities are associated with different molecular films used to support the receptor. Because these molecular films are electronically and electrostatically different, though slightly, the sensitiveness is influenced by these distinct characteristics. Nonetheless, the influence of target-to-receptor size ratio is significantly higher.

4. Conclusions

In this paper we demonstrated that the sensitivity of a mesoscopic electrochemical capacitive assay comprising of redox molecular films (containing biological receptors) is strongly based on target-to-receptor size ratio which is controlled by field effect characteristics of the interface. The target-to-receptor size ratio was verified in different molecular films composed of thiolated or peptide structures. As expected, receptive interfaces in which the target has a larger molecular weight than the receptor is demonstrated to have greater sensitivity than those in which a large receptor was used to detect small targets. The highest degree of sensitivity was observed in structures that were molecularly engineered to have the smallest possible receptor to detect the largest possible target. The limitations of these mesoscopic sensors are on the stability of the interface, which requires an accurate control of the molecular scale roughness of the interface. Future works are needed to a better understand of how the electronic structure of these electrochemical molecular junctions, in contact with different solvents, affects the field effect and sensitiveness.

Acknowledgements

We gratefully acknowledge the Royal Society and FAPESP (São Paulo Research Foundation) for their financial support. We would also like to warmly acknowledge graduate students, and especially Julia P. Piccolli, for procuring some of the peptides used in this study.

Declaration of interests

None.

Appendix A. Supporting information

Supplementary data associated with this article can be found in the online version at doi:10.1016/j.bios.2018.12.018.

References

Alcon, S., Talarmin, A., Debruyne, M., Falconar, A., Deubel, V., Flamand, M., 2002. Enzyme-linked immunosorbent assay specific to dengue virus type 1 nonstructural protein NS1 reveals circulation of the antigen in the blood during the experiencing primary acute phase of disease in patients or secondary infections. J. Clin. Microbiol. 40 (2), 376–381.

Ariga, K., Hill, J.P., Ji, Q.M., 2007. Layer-by-layer assembly as a versatile bottom-up nanofabrication technique for exploratory research and realistic application. Phys. Chem. Chem. Phys. 9 (19), 2319–2340.

Balasubramanian, K., Burghard, M., 2006. Biosensors based on carbon nanotubes. Anal. Bioanal. Chem. 385 (3), 452–468.

Bard, A.J., Faulkner, L.R., 2000. Electrochemical Methods Fundamentals and Applications, 2nd ed. John Wiley & Sons.

Bartic, C., Borghs, G., 2006. Organic thin-film transistors as transducers for (bio) analytical applications. Anal. Bioanal. Chem. 384 (2), 354–365.

Barton, B.E., 1997. IL-6: insights into novel biological activities. Clin. Immunol. Immunopathol. 85 (1), 16–20.

Berggren, M., Richter-Dahlfors, A., 2007. Organic bioelectronics. Adv. Mater. 19 (20), 3201–3213.

Bing, X.H., Wang, G.R., 2017. Label free C-reactive protein detection based on an electrochemical sensor for clinical application. Int. J. Electrochem. Sci. 12 (7), 6304–6314.

Bondy, C.R., Loeb, S.J., 2003. Amide based receptors for anions. Coord. Chem. Rev. 240 (1–2), 77–99.

Bradley, K., Briman, M., Star, A., Gruner, G., 2004. Charge transfer from adsorbed proteins. Nano Lett. 4 (2), 253–256.

Bueno, P.R., 2018. Common principles of molecular electronics and nanoscale electrochemistry. Anal. Chem. 90 (12), 7095–7106.

Bueno, P.R., Benites, T.A., Davis, J.J., 2016. The mesoscopic electrochemistry of molecular junctions. Sci. Rep. 6, 18400.
Bueno, P.R., Davis, J.J., 2014a. Elucidating redox-level dispersion and local dielectric effects within electroactive molecular films. Anal. Chem. 86 (4), 1997–2004.
Bueno, P.R., Davis, J.J., 2014b. Measuring quantum capacitance in energetically addressable molecular layers. Anal. Chem. 86 (3), 1337–1341.
Bueno, P.R., Feliciano, G.T., Davis, J.J., 2015. Capacitance spectroscopy and density functional theory. Phys. Chem. Chem. Phys. 17, 9375–9382.
Bueno, P.R., Fernandes, F.C.B., Davis, J.J., 2017. Quantum capacitance as a reagentless molecular sensing element. Nanoscale 9 (40), 15362–15370.
Büttiker, M., Thomas, A., Prêtre, A., 1993. Mesoscopic capacitors. Phys. Lett. A 180 (4–5), 364–369.
Cecchetto, J., Carvalho, F.C., Santos, A., Fernandes, F.C.B., Bueno, P.R., 2015. An impedimetric biosensor to test neat serum for dengue diagnosis. Sens. Actuator B-Chem. 213, 150–154.
Cecchetto, J., Fernandes, F.C.B., Lopes, R., Bueno, P.R., 2017. The capacitive sensing of NS1 Flavivirus biomarker. Biosens. Bioelectron. 87, 949–956.
Chen, J.N., Badioli, M., Alonso-Gonzalez, P., Thongrattanasiri, S., Huth, F., Osmond, J., Spasenovic, M., Centeno, A., Pesquera, A., Godignon, P., Elorza, A.Z., Camara, N., de Abajo, F.J.G., Hillenbrand, R., Koppens, F.H.L., 2012. Optical nano-imaging of gate-tunable graphene plasmons. Nature 487 (7405), 77–81.
Chen, Z.H., Lin, Y.M., Rooks, M.J., Avouris, P., 2007. Graphene nano-ribbon electronics. Phys. E-Low-Dimens. Syst. Nanostruct. 40 (2), 228–232.
de Ávila, B.E.-F., Escamilla-Gomez, V., Campuzano, S., Pedrero, M., Salvador, J.-P., Marco, M.-P., Pingarrón, J.M., 2013. Ultrasensitive amperometric magnetoimmunosensor for human C-reactive protein quantification in serum. Sens. Actuators B: Chem. 188, 212–220.
Eckermann, A.L., Feld, D.J., Shaw, J.A., Meade, T.J., 2010. Electrochemistry of redox-active self-assembled monolayers. Coord. Chem. Rev. 254 (15–16), 1769–1802.
Fernandes, F.C.B., Góes, M.S., Davis, J.J., Bueno, P.R., 2013. Label free redox capacitive biosensing. Biosens. Bioelectron. 50 (0), 437–440.
Fernandes, F.C.B., Patil, A.V., Bueno, P.R., Davis, J.J., 2015. Optimized diagnostic assays based on redox tagged bioreceptive interfaces. Anal. Chem. 87 (24), 12137–12144.
Friend, R.H., Gymer, R.W., Holmes, A.B., Burroughes, J.H., Marks, R.N., Taliani, C., Bradley, D.D.C., Dos Santos, D.A., Bredas, J.L., Logdlund, M., Salaneck, W.R., 1999. Electroluminescence in conjugated polymers. Nature 397 (6715), 121–128.
Grieshaber, D., MacKenzie, R., Voros, J., Reimhult, E., 2008. Electrochemical biosensors – sensor principles and architectures. Sensors 8 (3), 1400–1458.
Grosberg, A.Y., Nguyen, T.T., Shklovskii, B.I., 2002. Colloquium: the physics of charge inversion in chemical and biological systems. Rev. Mod. Phys. 74 (2), 329–345.
Gudiksen, M.S., Lauhon, L.J., Wang, J., Smith, D.C., Lieber, C.M., 2002. Growth of nanowire superlattice structures for nanoscale photonics and electronics. Nature 415 (6872), 617–620.
Guo, L., Yang, Z., Zhi, S.T., Feng, Z., Lei, C., Zhou, Y., 2018. A sensitive and innovative detection method for rapid C-reactive proteins analysis based on a micro-fluxgate sensor system. PLoS One 13 (3).
Gutierrez, F.A., Fernandes, F.C.B., Rivas, G.A., Bueno, P.R., 2017. Mesoscopic behaviour of multi-layered graphene: the meaning of supercapacitance revisited. Phys. Chem. Chem. Phys. 19 (9), 6792–6806.
Hanafi, H.I., Tiwari, S., Khan, I., 1996. Fast and long retention-time nano-crystal memory. IEEE Trans. Electron Devices 43 (9), 1553–1558.
Hudari, F.F., Bessegato, G.G., Bedatty Fernandes, F.C., Zanoni, M.V.B., Bueno, P.R., 2018. Reagentless detection of low-molecular-weight triamterene using self-doped TiO2 nanotubes. Anal. Chem. 90 (12), 7651–7658.
Kaempgen, M., Chan, C.K., Ma, J., Cui, Y., Gruner, G., 2009. Printable thin film supercapacitors using single-walled carbon nanotubes. Nano Lett. 9 (5), 1872–1876.
Landauer, R., 1992. Conductance from transmission – common-sense points. Phys. Scr. T42, 110–114.
Lange, U., Roznyatouskaya, N.V., Mirsky, V.M., 2008. Conducting polymers in chemical sensors and arrays. Anal. Chim. Acta 614 (1), 1–26.
Lehr, J., Fernandes, F.C.B., Bueno, P.R., Davis, J.J., 2014. Label-free capacitive diagnostics: exploiting local redox probe state occupancy. Anal. Chem. 86 (5), 2559–2564.
Lehr, J., Weeks, J.R., Santos, A., Feliciano, G.T., Nicholson, M.I.G., Davis, J.J., Bueno, P.R., 2017. Mapping the ionic fingerprints of molecular monolayers. Phys. Chem. Chem. Phys.
Levin, Y., 2002. Electrostatic correlations: from plasma to biology. Rep. Prog. Phys. 65 (11), 1577–1632.
Lin, P., Yan, F., 2012. Organic Thin-Film Transistors for Chemical and Biological Sensing. Adv. Mater. 24 (1), 34–51.
Luryi, S., 1988. Quantum capacitance devices. Appl. Phys. Lett. 52, 501.
Mabeck, J.T., Malliaras, G.G., 2006. Chemical and biological sensors based on organic thin-film transistors. Anal. Bioanal. Chem. 384 (2), 343–353.
Marques, S.M., Santos, A., Goncalves, L.M., Sousa, J.C., Bueno, P.R., 2015. Sensitive label-free electron chemical capacitive signal transduction for D-dimer electroanalysis. Electrochim. Acta 182, 946–952.
McAlpine, M.C., Ahmad, H., Wang, D.W., Heath, J.R., 2007. Highly ordered nanowire arrays on plastic substrates for ultrasensitive flexible chemical sensors. Nat. Mater. 6 (5), 379–384.
McCulloch, I., Heeney, M., Bailey, C., Genevicius, K., Macdonald, I., Shkunov, M., Sparrowe, D., Tierney, S., Wagner, R., Zhang, W.M., Chabinyc, M.L., Kline, R.J., McGehee, M.D., Toney, M.F., 2006. Liquid-crystalline semiconducting polymers with high charge-carrier mobility. Nat. Mater. 5 (4), 328–333.
Miranda, D.A., Bueno, P.R., 2016. Density functional theory and an experimentally-designed energy functional of electron density. Phys. Chem. Chem. Phys. 18 (37), 25984–25992.
Ohno, Y., Maehashi, K., Yamashiro, Y., Matsumoto, K., 2009. Electrolyte-gated graphene field-effect transistors for detecting pH protein adsorption. Nano Lett. 9 (9), 3318–3322.
Parkash, O., Hanim Shueb, R., 2015. Diagnosis of dengue infection using conventional and biosensor based techniques. Viruses-Basel 7 (10), 5410–5427.
Piccoli, J., Hein, R., El-Sagheer, A.H., Brown, T., Cilli, E.M., Bueno, P.R., Davis, J.J., 2018. Redox capacitive assaying of C-reactive protein at a peptide supported aptamer interface. Anal. Chem. 90 (5), 3005–3008.
Rosenblatt, S., Yaish, Y., Park, J., Gore, J., Sazonova, V., McEuen, P.L., 2002. High performance electrolyte gated carbon nanotube transistors. Nano Lett. 2 (8), 869–872.
Santos, A., Carvalho, F.C., Roque-Barreira, M.C., Bueno, P.R., 2014. Impedance-derived electrochemical capacitance spectroscopy for the evaluation of lectin-glycoprotein binding affinity. Biosens. Bioelectron. 62, 102–105.
Santos, A., Piccoli, J.P., Santos-Filho, N.A., Cilli, E.M., Bueno, P.R., 2015. Redox-tagged peptide for capacitive diagnostic assays. Biosens. Bioelectron. 68, 281–287.
Singh, V., Joung, D., Zhai, L., Das, S., Khondaker, S.I., Seal, S., 2011. Graphene based materials: past, present and future. Prog. Mater. Sci. 56 (8), 1178–1271.
Vanderspiegel, J., Lauks, I., Chan, P., Babic, D., 1983. The extended gate chemically sensitive field-effect transistor as multi-species microprobe. Sens. Actuators 4 (2), 291–298.
Wang, Z.L., 2004. Functional oxide nanobelts: materials, properties and potential applications in nanosystems and biotechnology. Annu. Rev. Phys. Chem. 55, 159–196.
Yang, X., Wang, Y., Wang, K., Wang, Q., Wang, P., Lin, M., Chen, N., Tan, Y., 2014. DNA aptamer-based surface plasmon resonance sensing of human C-reactive protein. RSC Adv. 4, 30934–30937.